Petroleum Science 23 (2026) 1459–1468

Contents lists available at ScienceDirect

Petroleum Science

journal homepage: www.keaipublishing.com/en/journals/petroleum-science

Original Paper

Charge-structure synergy in reservoir wettability reversal: Investigating with an integrated optical-multiscale framework

Chao Song [a,b], Yi-Qin Yang [c], Wen-Ya Zhang [d], Xin Liu [b], Zhi-Yuan Xu [a], Ke-Xin Li [b], Hao Zhang [b], Chun-Qing Si [b], Si-Hao Ma [b], Jia-Ning Zhang [b], Yan-Yan Wang [b], Bo-Wen Sun [b], Sheng-Nan Wu [a], Mei-Yi Qing [e], Qi-Chao Lv [a], Jing Wang [a], Hong-Lei Zhan [a,b,*]

[a] State Key Laboratory of Petroleum Resources and Engineering, China University of Petroleum (Beijing), Beijing, 102249, China
[b] College of New Energy and Materials, China University of Petroleum (Beijing), Beijing, 102249, China
[c] Key Laboratory of Clean Conversion and High Value Utilization of Biomass Resources in Xinjiang, School of Chemistry and Chemical Engineering, Yili Normal University, Yining, 835000, Xinjiang, China
[d] No. 2 Mud Logging Company, BHDC, CNPC, Renqiu, 062552, Hebei, China
[e] School of Electronic and Electrical Engineering, Chongqing University of Science and Technology, Chongqing, 401331, China

ARTICLE INFO

Article history:
Received 19 July 2025
Received in revised form
6 November 2025
Accepted 9 November 2025
Available online 13 November 2025

Edited by Yan-Hua Sun

Keywords:
Wettability alteration
Solid–liquid interface
Oblique-incidence reflectivity difference (OIRD)
Dielectric constant
Interface thickness
Multiscale characterization

ABSTRACT

Reservoir wettability modification is a key strategy for enhancing oil recovery (EOR), yet the mechanisms driving this reversal remain incompletely understood due to the scarcity of multiscale characterization methods. In this study, we developed an integrated multiscale framework that combines contact angle measurements, rheological analysis, quartz crystal microbalance with dissipation monitoring (QCM-D), and oblique-incidence reflectivity difference (OIRD) to investigate surfactant-mediated wettability reversal. Our findings reveal distinct charge-dependent pathways: anionic sodium dodecyl sulfate (SDS) promotes monotonic hydrophilization through hydrophobic-driven monolayer adsorption. In contrast, cationic cetyltrimethylammonium bromide (CTAB) exhibits a non-monotonic wettability transition—initially increasing hydrophobicity before sharply reversing to a hydrophilic state. This behavior arises from initial electrostatic adsorption forming hydrophobic monolayers, followed by post-critical micelle concentration (post-CMC) micellar co-adsorption, a process involving interfacial integration and reorganization of surfactant micelles that culminates in bilayer formation and hydrophilic reversal. CTAB's cationic groups enable strong electrostatic anchoring to negatively charged mica substrates, facilitating dense monolayer-to-bilayer transitions. Conversely, SDS anionic headgroups experience electrostatic repulsion, limiting adsorption to disordered monolayers. This multiscale approach offers critical mechanistic insights for optimizing functional coatings and microfluidic systems via precise wettability control.

1. Introduction

Wettability is a critical property of solid surfaces (Liu et al., 2019). It plays a vital role in numerous engineering and technological fields, including biomimetic material design, enhanced oil recovery, oil–water separation, microfluidic systems, anti-fouling and anti-corrosion coatings, micro-nano fabrication, and biomedical engineering (Samiei et al., 2021; Shi et al., 2024; Wang et al., 2023; Yao et al., 2021; Zhang et al., 2017; Zhang and Zeng, 2021). Wettability reflects the dynamic process wherein the solid–gas interface is replaced by the solid–liquid interface, with extensive research demonstrating that it is fundamentally determined by the chemical composition and microstructural morphology of material surfaces (Ghasemlou et al., 2019; Huang et al., 2023). Young's equation establishes the equilibrium relationship between the contact angle on an ideal smooth surface and the three-phase interfacial tensions. To address the roughness characteristics of practical engineering surfaces, the Wenzel model introduces surface roughness factors to modify contact angle

*Corresponding author.
E-mail address: zhanhl@cup.edu.cn (H.-L. Zhan).
Peer review under the responsibility of China University of Petroleum (Beijing).

https://doi.org/10.1016/j.petsci.2025.11.021

calculations. Furthermore, the Cassie–Baxter model constructs a mathematical framework for gas–liquid phase coexistence under composite wetting states (Sbragaglia et al., 2006). Building upon these theoretical foundations, modern surface engineering enables precise modulation of material wettability through surface chemical modification and microstructure design (Wang et al., 2024).

In petroleum engineering, wettability alteration serves as a fundamental method for enhanced oil recovery (EOR) (Roldán-Carrillo et al., 2023). This technique enhances crude oil recovery by modifying reservoir rock surfaces from oil-wet to water-wet states, securing its pivotal role in EOR strategies (Ratanpara and Kim, 2023). Surfactant flooding is the primary method for achieving wettability alteration in EOR. Surfactants are amphiphilic molecules, characterized by a hydrophilic headgroup and a hydrophobic tail. This structure grants them unique interfacial activity (Yao et al., 2021). The surface charges of reservoir rocks vary; carbonate reservoirs are typically positively charged, while sandstones are negatively charged. Surfactants modify wettability through three main mechanisms: ion-pair formation, selective adsorption, and micellization (Hou et al., 2015).

Comparative studies of surfactant-mediated wettability alteration reveal distinct mechanistic variations across surfactant types and mineral substrates (Esfandyari et al., 2020). The anionic surfactant sodium dodecyl benzene sulfonate (SDBS) demonstrates superior wettability reversal capability for carbonate minerals and quartz surfaces, effectively converting strongly oil-wet surfaces to neutral or weakly water-wet states. Multiscale investigations of gemini surfactant (GABEO, a gemini surfactant) elucidate its enhanced performance in oil-wet sandstone systems, where nuclear magnetic resonance (NMR) and infrared spectroscopy (IR) confirm successful synthesis and a robust ion-desorption mechanism that reduces asphaltene adsorption by 30%–45% compared to conventional surfactants dodecyltrimethylammonium bromide (DTAB) and didodecyltrimethylammonium bromide (GDTAB) (Hou et al., 2019). Spontaneous imbibition experiments further validate GABEO's optimal recovery efficiency, attributed to synergistic interactions between hydrophilic/hydrophobic groups that destabilize crude oil–rock interfacial layers, providing molecular insights for smart flooding agent design. Systematic analyses integrating contact angle measurements, FTIR, EDX, and SEM (Mousavi et al., 2021) identify asphaltenes as the dominant primary factor of carbonate wettability, with oil-aged surfaces exhibiting pronounced organic enrichment (contact angle increase: asphaltenes > resins). Nanocomposite treatments leveraging structural disjoining pressure gradients effectively restore hydrophilicity by displacing adsorbed oil phases. Additionally, based on the studies of surfactant mixtures for wettability alteration, the benzimidazolium gemini surface-active ionic liquid (GSAIL)/SDS blend demonstrated direct and superior performance in transforming oil-wet surfaces to water-wet with a 72.8% synergistic efficiency. In contrast, while the imidazolium surface-active ionic liquid (SAIL)/SDS mixture showed strong synergy in reducing IFT and critical micelle concentration (CMC), its specific impact on wettability was not explicitly measured. These findings collectively confirm that cationic SAIL/anionic surfactant pairs are highly effective for synergistic interfacial property enhancement (Asadabadi et al., 2024; Saien et al., 2023).

Significant knowledge gaps persist in fundamentally correlating macroscopic wettability with its nanoscopic origins. While extensive research has characterized both macroscopic contact angles and molecular-scale interactions, a critical disconnect remains in quantitatively linking these different scales. This is particularly evident in surfactant-mediated systems, where experimental data often show significant scatter and apparent contradictions (Pal et al., 2018; Zhang et al., 2023), primarily due to the inability to directly connect real-time interfacial molecular reorganization with consequent macroscopic wetting transitions. The core challenge lies in the multiscale nature of wettability: macroscopic measurements lack nanoscale resolution, while high-resolution techniques often operate under conditions far from practical scenarios or cannot directly link their signals to macroscopic properties. Although computational simulations provide valuable insights, their accuracy is constrained by empirical parameters. Thus, a methodology capable of seamlessly bridging the macro-nano scale gap is crucially needed. To address this fundamental challenge, this study introduces an integrated optical-multiscale framework whose novelty lies in directly connecting macroscopic wettability with nanoscopic interfacial properties. Applying our framework to well-characterized surfactant models successfully reveals how headgroup charge dictates interfacial adsorption structures and wettability pathways. Our framework uniquely combines contact angle measurements (macroscopic wettability), interfacial rheology (bulk properties), and most importantly, simultaneously employs QCM-D and high-resolution OIRD (< 1 nm *z*-resolution) (Zhu, 2004) to provide complementary nanoscale information on adsorbed mass, viscoelasticity, interfacial thickness and dielectric constant (Meng et al., 2023; Qing et al., 2022). This multi-technique integration enables us to directly correlate nanoscopic interfacial transformations, monitored in real-time, with the resulting macroscopic contact angle evolution, thereby elucidating the fundamental mechanisms governing wettability alteration.

2. Experimental

2.1. Experimental materials

This study employed two conventional ionic surfactants (Fig. 1): sodium dodecyl sulfate (SDS, anionic, molecular weight 288.4, purity ≥ 99.0 %) and cetyltrimethylammonium bromide (CTAB, cationic, molecular weight 364.5, purity ≥ 99.0 %). Mica, a layered aluminosilicate mineral ($KAl_2(AlSi_3O_{10})(OH)_2$), was selected as a model substrate due to its well-defined crystalline structure, surface properties analogous to reservoir clay minerals, and mechanically cleavable extremely flat surfaces that provide an ideal platform for studying surfactant-induced wettability transitions while minimizing natural rock heterogeneity.

2.2. Experimental methods

The oblique-incidence reflectivity difference (OIRD) technique, based on polarized light modulation, is a high-sensitivity surface analysis method. As illustrated in Fig. 2(a), a linearly polarized laser beam (632.8 nm wavelength) irradiates the sample surface at the Brewster angle. The interfacial properties are characterized by detecting differential changes in reflectivity coefficients between s-polarized and p-polarized light. According to Fresnel equations, under oblique laser incidence, the reflectivity difference between

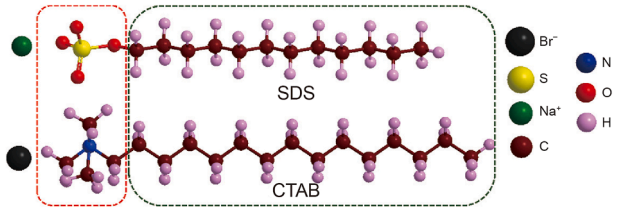

Fig. 1. Molecular structures of SDS and CTAB.

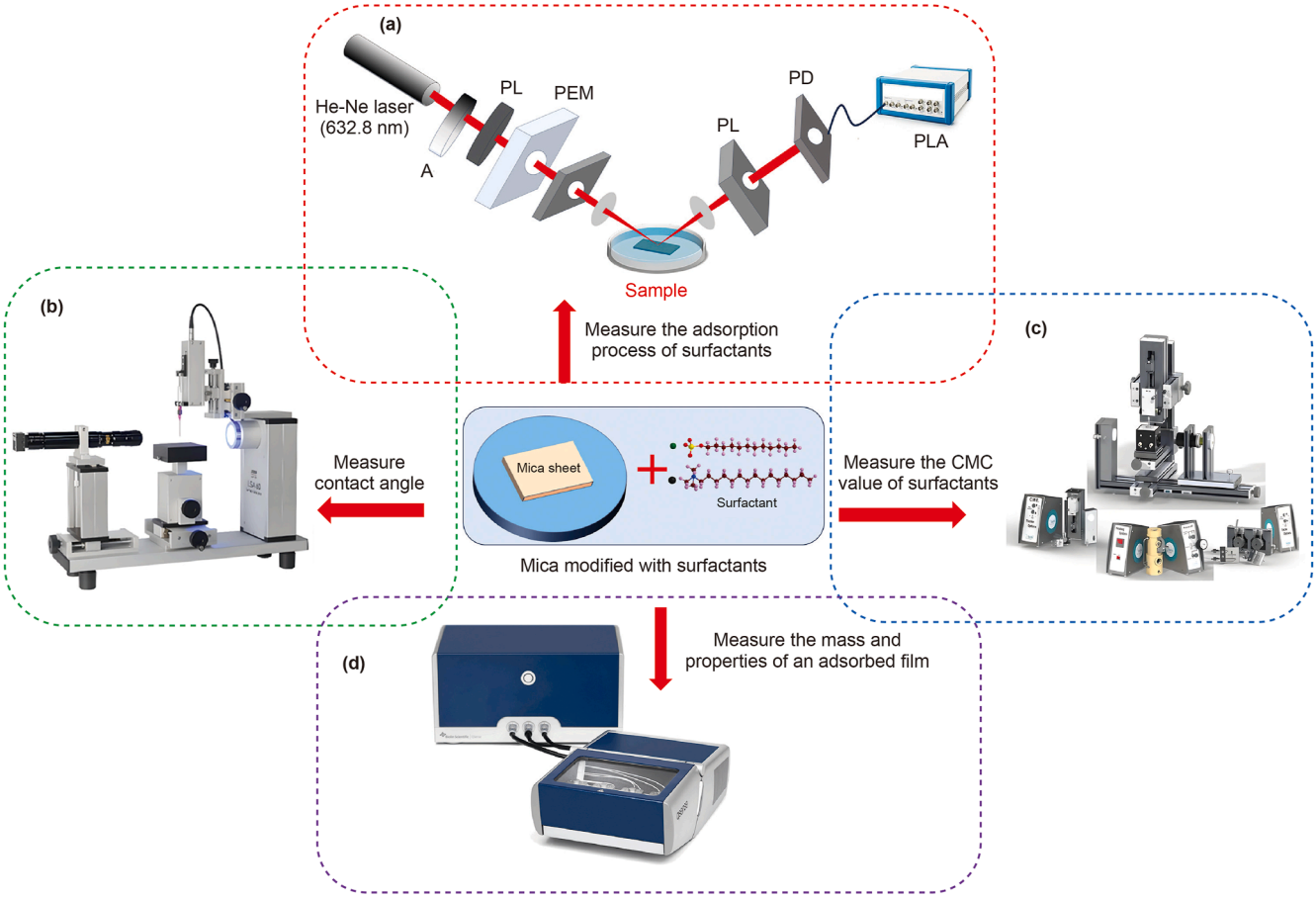

Fig. 2. Schematic diagrams of experimental methodologies: (**a**) OIRD device and testing schematic diagram, (**b**) contact angle measurement instrument, (**c**) interfacial rheometer, (**d**) quartz crystal microbalance with dissipation monitoring.

s-polarizations and p-polarizations is directly correlated with variations in the interfacial layer's dielectric constant or thickness. The dielectric constant (ε) characterizes a material's polarizability under an electric field, representing its capacity to store electrical energy. In the context of OIRD measurements, changes in ε reflect variations in molecular density, orientation, and electronic structure at the interface. Since this parameter intrinsically relates to surface molecular packing, orientation, and electronic properties, while simultaneously, the adsorption layer thickness (d) reflects nanoscale molecular adsorption and conformational changes, the OIRD system employs dual-channel lock-in amplification to precisely demodulate differential signals. This integrated approach enables real-time dynamic monitoring of molecular behavior at solid/liquid interfaces, providing comprehensive insights into surfactant adsorption mechanisms and layer reorganization.

For wettability analysis, an imaging-analysis-based contact angle measurement system was employed. As shown in Fig. 2(b), a 4 μL deionized water droplet was precisely deposited onto the mica substrate using a microsyringe. A CCD high-speed camera system equipped with a zoom microscopic objective recorded the dynamic evolution of the three-phase contact line. The equilibrium contact angle (θ) was determined via numerical fitting of the Young–Laplace equation using edge detection algorithms to extract droplet contour features. The system achieved an angular resolution of ±0.1°, with a temperature-controlled stage (±0.1 °C) ensuring experimental consistency.

The Teclis Tracker interfacial rheometer was utilized to establish a droplet expansion rheology analysis system for CMC measurement. As depicted in Fig. 2(c), dual syringe pumps precisely controlled periodic oscillations of the gas/water interfacial area, enabling real-time morphological parameter extraction. By solving the modified Young–Laplace equation, dynamic interfacial tension and viscoelastic parameters were simultaneously acquired. Upon reaching the CMC, interfacial adsorption saturation was observed, characterized by a decrease in interfacial tension to a stable value.

The adsorption behavior of CTAB and SDS on silica chip surfaces was characterized using a dissipation quartz crystal microbalance (QCM-D), as illustrated in Fig. 2(d). The core principle involved utilizing the piezoelectric effect of the quartz crystal to induce high-frequency vibration. When substances adsorbed onto the crystal surface, a decrease in vibration frequency occurred, allowing the adsorbed mass to be calculated. Additionally, QCM-D was capable of measuring the dissipation of vibrational energy. A faster energy decay indicated a softer adsorbed layer, while a slower decay suggested a more rigid layer. By monitoring the frequency shift (Δf) and dissipation shift (ΔD) in real time during the adsorption process, QCM-D revealed the mass, thickness, and structural morphology of the adsorbates. This approach was employed to compare the adsorption differences between an anionic surfactant (SDS) and a cationic surfactant (CTAB) on solid surfaces. The experimental work was conducted under a resonance frequency of 15 MHz and a constant temperature of 25 °C.

2.3. Experimental protocols

Throughout the OIRD measurements, fixed-point detection was employed to ensure measurement stability and minimize interfacial

disturbances. Freshly cleaved mica surfaces were prepared by mechanical exfoliation using precision tweezers immediately before each experiment. The prepared mica sheet was placed in a 100 mm-diameter glass Petri dish with the cleavage plane facing upward and then rigidly mounted on the sample stage to prevent movement during measurements, as illustrated in Fig. 2(a). After adding deionized water, a translation stage was used to precisely align the incident beam spot with the target location on the mica surface. Upon completing optical alignment, the sample remained immobilized to maintain consistent beam coverage throughout the experiment. OIRD signals were continuously acquired from this fixed point during testing. Surfactant concentrations were incrementally increased via syringe injection at a site sufficiently distant from the detection point to avoid local hydrodynamic disruption, until predetermined concentration levels were reached.

Contact angle characterization was performed using a goniometer equipped with a thermostatic stage (25.0±0.5 °C). Prior to measurement, the mica substrates were modified by immersing freshly cleaved sheets in surfactant solutions of varying concentrations for 15 h, followed by air-drying at room temperature. A 4 μL ultrapure water droplet was deposited onto modified mica substrates via a microinjection pump at a dynamic deposition rate of 0.5 μL/s. High-speed imaging captured wetting kinetics post-deposition. Equilibrium contact angles were computed using a modified elliptical fitting algorithm applied to droplet contours, with static contact angles recorded as quantitative wettability indicators.

For interfacial tension measurements, surfactant solutions of varying concentrations were loaded into quartz cuvettes. A bent syringe filled with air was vertically positioned above the cuvette, with the needle tip submerged until barely visible in the monitoring interface. Motorized syringe actuation generated air bubbles, establishing air/surfactant solution interfaces. Software-controlled bubble volume adjustments enabled precise interfacial area modulation, with automatic interfacial tension calculations via real-time Young–Laplace equation solutions. The testing interface permitted simultaneous monitoring of bubble morphology (area/volume), attachment status, and dynamic interfacial tension.

Owing to their considerable thickness and surface irregularity, natural mica sheets were deemed unsuitable for direct measurement with a quartz crystal microbalance with dissipation monitoring (QCM-D). Since the primary components of mica are silica and alumina, and a silica surface carries a negative charge under neutral or alkaline pH conditions, standard silica sensor chips—which were flatter and possessed a surface charge comparable to that of mica—were selected as substitutes in this study. The adsorption behavior of the surfactants, sodium dodecyl sulfate (SDS) and cetyltrimethylammonium bromide (CTAB), onto the silica surface was investigated using QCM-D. Experimentally, a silica sensor chip was first mounted in the flow chamber, and ultrapure water was introduced to establish a stable baseline. Subsequently, solutions of different concentrations of SDS or CTAB, dissolved in the same background electrolyte, were sequentially perfused through the system. The concomitant changes in the quartz crystal's Δf and ΔD were monitored in real time. Following the achievement of adsorption equilibrium at each concentration, a buffer rinse was performed to assess the reversibility of the adsorption process. A new silica sensor chip was employed for each concentration to ensure data integrity. By analyzing the temporal profiles of Δf and ΔD, the differences in adsorbed mass and adsorption layer structure between the two surfactants on the negatively charged silica surface, which arose from their distinct electrical properties, were elucidated.

3. Results and discussion

3.1. Surfactant-mediated wettability modification of mica substrates

Fig. 3(a) and (b) reveal distinct concentration-dependent wettability responses of mica surfaces modified with anionic/cationic surfactants. Fig. 3(c) and (d) present the contact angle profiles of SDS and CTAB, respectively, on mica surfaces at various concentrations. As shown in Fig. 3(a), the equilibrium contact angle (θ) of the SDS-modified system decreased monotonically with increasing SDS concentration (0–50.0 mmol/L). In the range of 0–10.0 mmol/L, θ sharply declined from 32° to 14.6°, indicating a significant reduction in solid–liquid interfacial energy due to surfactant adsorption. Beyond 10 mmol/L (approaching SDS's critical micelle concentration, CMC = 9.5 mmol/L), the θ reduction rate diminished, demonstrating dynamic adsorption equilibrium at the interface. In contrast, the CTAB system exhibited non-monotonic wettability behavior (Fig. 3(b)). Within 0–0.8 mmol/L, θ increased quasi-linearly with CTAB concentration, correlating with hydrophobic monolayer formation via electrostatic interactions between

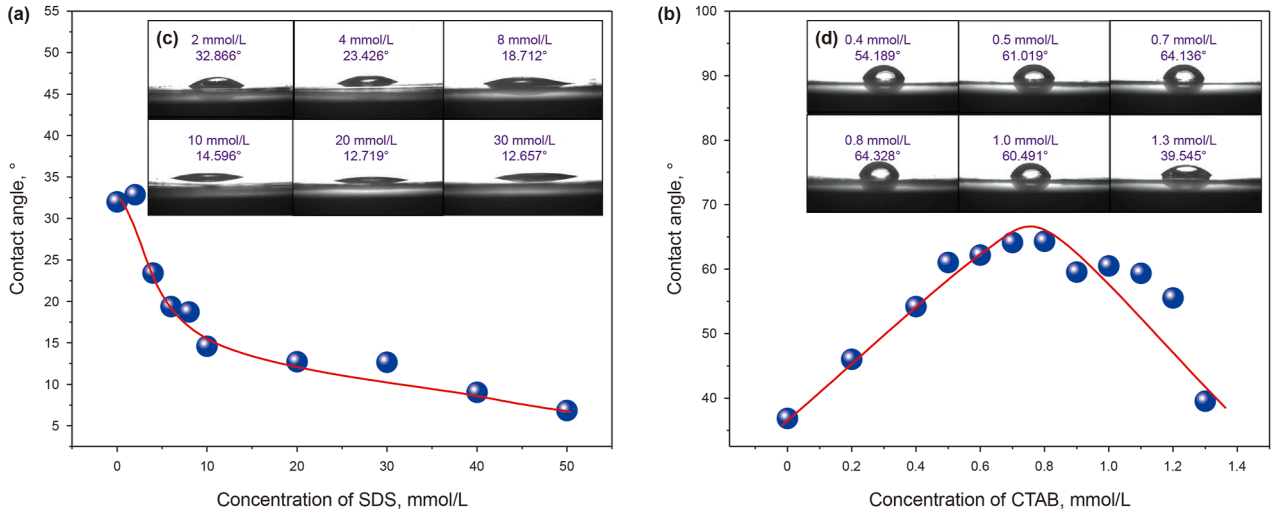

Fig. 3. Contact angle evolution on mica surfaces modified with sodium dodecyl sulfate (SDS) (**a, c**) and cetyltrimethylammonium bromide (CTAB) (**b, d**).

cationic headgroups and the negatively charged mica surface. Upon exceeding 0.8 mmol/L (near CTAB's CMC = 1.0 mmol/L), θ underwent a marked reversal. This transition likely originated from micellization-driven surface charge inversion and interfacial exposure of hydrophilic moieties. The divergent evolutionary pathways between the two systems underscored the distinct regulatory mechanisms of surfactant molecular architecture and substrate charge properties on interfacial wettability.

3.2. Determination of critical micelle concentration (CMC) of surfactants

Fig. 4 compares the concentration-dependent surface tension (γ) profiles of anionic (SDS) and cationic (CTAB) surfactant systems. For the CTAB system (Fig. 4), within the pre-micellar concentration regime (0–1.0 mmol/L), γ exhibited exponential decay, consistent with the interfacial molecular alignment process governed by the Gibbs adsorption equation. At the critical micelle concentration (CMC = 1.0 mmol/L), γ stabilized at 33.1±0.3 mN/m, indicating monolayer saturation at the air/liquid interface.

In contrast, the SDS system (Fig. 4) exhibited a wider pre-micellar range (0–9.5 mmol/L) with a nonlinear γ–C profile. In the low-concentration regime (0–5.0 mmol/L), the gradual reduction in γ reflected hindered adsorption kinetics at the air/water interface, attributed to electrostatic repulsion between anionic headgroups. Near the CMC (9.5 mmol/L), an inflection point emerged, indicating a transition in interfacial packing associated with micelle nucleation. Post-CMC ($C > 10.0$ mmol/L), γ stabilized at 24.8±0.2 mN/m. The higher equilibrium γ compared to CTAB was attributed to with the stronger hydration energy of anionic headgroups.

3.3. OIRD interrogation of surfactant adsorption states and mechanisms on mica

Based on the correlation between the intrinsic properties of surfactant solutions and their interfacial behavior, OIRD technology successfully captured the differential response characteristics of anionic/cationic surfactant adsorption at the mica/solution interface (Fig. 5). For SDS, the results revealed a biphasic concentration dependence: an exponential decay was observed between 0 and 10 mmol/L, followed by signal stabilization (amplitude = 0.052) within the concentration range of 10–50 mmol/L. In contrast, CTAB exhibited a triphasic response: a linear decrease occurred between

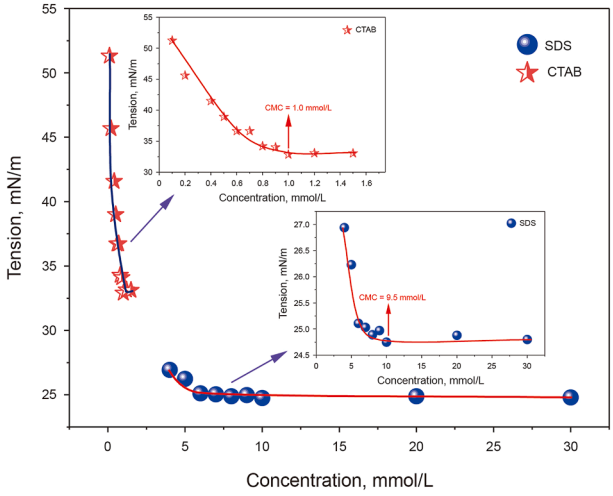

Fig. 4. Surface tension (γ) evolution of SDS and CTAB solutions as a function of surfactant concentration (C).

0 and 0.4 mmol/L; from 0.4 to 1.0 mmol/L, the decay rate decreased with signal attenuation slowing; and between 1.0 and 1.3 mmol/L, the signal increased markedly to 0.038. The distinct OIRD responses to the adsorption of these two surfactants on mica generated significant interest for further investigation. To better elucidate the differential adsorption behavior and underlying mechanisms, Fig. 5(c) and (d) were introduced. These figures were generated using a three-layer optical model formula, which defined the OIRD signal as a function of the interfacial layer's thickness (d) and dielectric constant (ε_d). According to the Fresnel equations, when the sample thickness was much smaller than the laser wavelength ($d \ll \lambda$), the OIRD definition simplified to

$$\Delta p - \Delta s = \frac{(-i)4\pi d\sqrt{\varepsilon_0}\varepsilon_s \cos\phi_{inc}\sin^2\phi_{inc}}{\lambda(\varepsilon_s - \varepsilon_0)\left(\varepsilon_s\cos^2\phi_{inc} - \varepsilon_0\sin^2\phi_{inc}\right)} \frac{(\varepsilon_d - \varepsilon_0)(\varepsilon_d - \varepsilon_s)}{\varepsilon_d}$$

where ϕ_{inc} is the incident angle of the detection laser; d is the interface thickness; ε_0, ε_d, and ε_s are the dielectric constants of the upper, interface, and lower layers, respectively. In Fig. 5(c), the dependence of the OIRD signal on ε_d was simulated by fixing the interfacial thickness and varying ε_d. The influence of dielectric constant demonstrated non-monotonic behavior, reaching maximum signal intensity at $\varepsilon_d = 24.3$. In Fig. 5(d), with ε_d fixed and d varied, the OIRD signal intensity exhibited a linear positive correlation with the d of the adsorption layer.

For the SDS system, within the concentration range of 0–10.0 mmol/L, the OIRD signal attenuation primarily originated from dielectric parameter modulation. Monolayer adsorption of dodecyl sulfate ions ($\varepsilon \approx 3.1$) on the mica surface reduced the effective interfacial dielectric constant ($\varepsilon \approx 7.3$, while SDS dielectric constant < 4, corresponding to the left side of the peak in Fig. 5(c)). When the concentration exceeded the CMC (10.0 mmol/L), micelle formation stabilized the dielectric constant while thickness variations became negligible, consistent with the observed adsorption saturation. The CTAB system exhibited a more complex dual-parameter coupling mechanism: in the range of 0–0.4 mmol/L stage, strong electrostatic interactions between cationic headgroups and the negatively charged mica surface caused ultrafast adsorption, leading to a sharp reduction in interfacial dielectric constant, where dielectric modulation dominated (similar to low-concentration SDS); in the range of 0.4–1.0 mmol/L, alkyl chain rearrangement formed a dense monolayer, reducing the signal decay rate; upon exceeding the CMC (1.0 mmol/L), the formation of micellar aggregates increased the adsorption layer thickness from a monolayer to approximately a bilayer (~6 nm) (Zhao et al., 2005), with thickness-driven signal intensification. This phenomenon revealed the dynamic competition between dielectric and thickness effects during surfactant self-assembly. The stark contrast between the simple dielectric-dominated response of SDS and the distinct thickness-dominated signal intensification observed for CTAB underscores how surfactant headgroup charge dictates the interfacial adsorption pathway.

3.4. QCM-D characterization of surfactant adsorption on a silica surface

For the anionic surfactant SDS, only weak QCM-D signal responses were elicited within the concentration range of 2.0–15.0 mmol/L. As depicted in Fig. 6, the Δf shifts were minimal, gradually increasing from −4.7 to −66.8 Hz, suggesting a limited increase in adsorbed mass. The corresponding ΔD values remained below 6.9×10^{-6}, indicating the formation of a very thin and rigid adsorption layer. Notably, after adsorption equilibrium was achieved at each concentration, rinsing with ultrapure water resulted

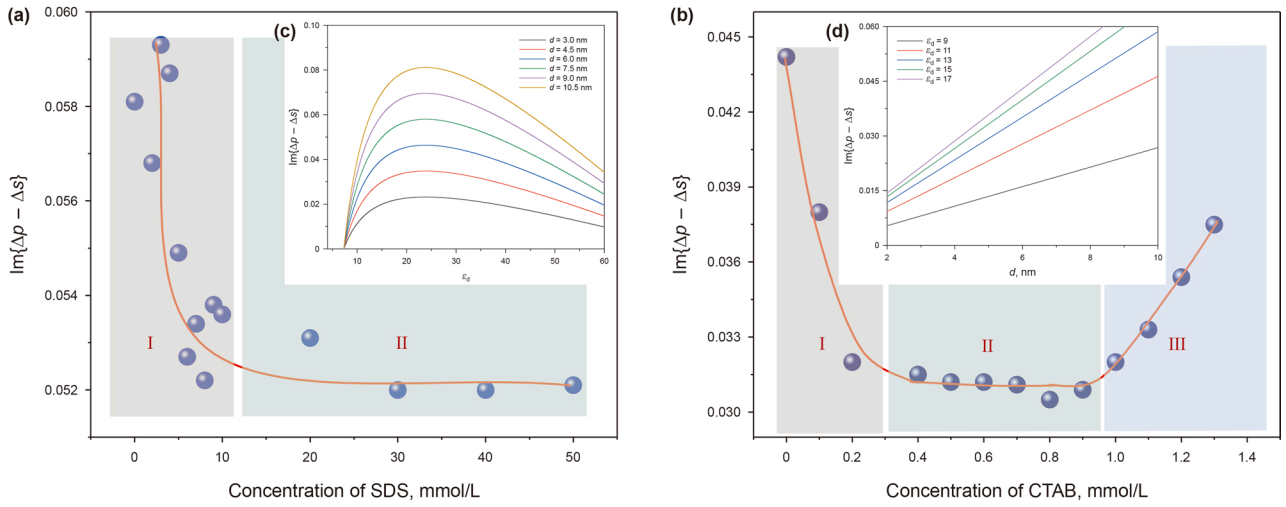

Fig. 5. Variation of the OIRD signal with surfactant solution concentration: (**a**) OIRD signal versus SDS concentration, (**b**) OIRD signal versus CTAB concentration, (**c**) simulation diagram of the relationship between the interfacial dielectric constant and OIRD signal, (**d**) simulation diagram of the relationship between the interface thickness and OIRD signal.

in a complete return of both Δf and ΔD signals to their baseline levels (Fig. 6). This observation demonstrated that the adsorption of SDS on the negatively charged mica surface was weak and fully reversible. The underlying cause lies in the strong electrostatic repulsion between the anionic headgroup of SDS and the mica surface, which considerably suppressed adsorption. Even if limited physisorption occurred at higher concentrations via hydrophobic interactions, the binding was exceedingly weak and susceptible to desorption during rinsing, thereby preventing the formation of a stable adsorption structure.

For the cationic surfactant CTAB, its adsorption behavior exhibited strong concentration dependence and markedly distinct characteristics (Fig. 7). In the low-concentration regime (0.2−0.8 mmol/L), Δf decreased from −4.5 to −46.1 Hz, while ΔD increased from 0.55×10^{-6} to 5.3×10^{-6}, consistent with the formation of a monolayer via electrostatic interactions. As the concentration approached and reached its critical micelle concentration (CMC = 1.0 mmol/L), the adsorption behavior underwent a sharp transition: both Δf and ΔD increased by orders of magnitude, reaching −825.2 Hz and 106.1×10^{-6}, respectively. This substantial change signified a fundamental transformation of the adsorption layer from a monolayer to a bilayer/micellar structure. Beyond the CMC (at 1.2 mmol/L), Δf and ΔD further increased to −917.3 Hz and 119.6×10^{-6}, indicating saturation of the adsorbed layer. In stark contrast to SDS, rinsing with ultrapure water following CTAB adsorption demonstrated strongly irreversible binding: Δf and ΔD showed only minor recovery and failed to return to baseline, with signals remaining nearly unchanged post-CMC (Fig. 7(c) and (d)). This strongly suggests that the primary CTAB layer, formed via strong electrostatic attraction, is highly stable, while the subsequent layer or surface aggregates, which are stabilized by hydrophobic interactions, also exhibit high robustness. This two-stage process collectively results in the formation of a rigid, viscoelastic bilayer adsorption structure.

3.5. Elucidation of charge-dependent adsorption mechanisms

Drawing upon the cross-scale information provided by contact angle, OIRD, and QCM-D measurements, this study constructed distinct models for the adsorption and wettability reversal mechanisms of anionic SDS and cationic CTAB at the mica-solution interface. The fundamental driving force originated from the difference in electrostatic interactions between the surfactant headgroup charge and the negatively charged mica substrate, which directly dictated the adsorption configuration, the evolution pathway of the layered structure, and the ultimate macroscopic wettability.

For the SDS system (Fig. 8(a)), the wettability evolution followed a monotonic hydrophilization pathway, governed fundamentally by electrostatic repulsion between its anionic headgroups and the negatively charged mica surface. This process was delineated into three distinct stages in Fig. 8(a). In the initial adsorption stage, SDS molecules adsorbed onto the mica surface via hydrophobic interactions, adopting a “tail-on” configuration. The primary effect in this stage was a significant reduction in the interfacial dielectric constant, which was directly evidenced by the characteristic decay in the OIRD signal (Fig. 5(a)). The subsequent stage, from adsorption saturation to pre-micelle formation, was characterized by the saturation of the adsorption sites, leading to the formation of a stable, sparse monolayer. During this stage, the interfacial dielectric constant remained largely unchanged, indicated by the stabilization of the OIRD signal, while the contact angle continued its gradual decrease (Fig. 3(a)) due to the now complete surface coverage. QCM-D data (Fig. 6) from these first two stages confirmed the formation of a thin, rigid adsorption layer with low adsorbed mass. Finally, in the post-micelle formation stage ($C \geq$ CMC), micelles formed in the bulk solution, but the persistent electrostatic barrier prevented any further cooperative adsorption or structural evolution at the interface. Both the OIRD signal and QCM-D measurements confirmed the absence of further changes, with no adsorption layer thickening observed. The complete reversibility of the QCM-D signal upon rinsing confirmed the entire process as weak, reversible physisorption. Consequently, the SDS-induced wettability alteration was constrained to a monotonic hydrophilization process, limited to a stable, low-density monolayer coverage.

For the CTAB system (Fig. 8(b)), the adsorption mechanism and wettability evolution demonstrated pronounced complexity, characterized by a strong, irreversible, and structurally transformative interfacial process. Both QCM-D (Fig. 7) and OIRD (Fig. 5(b)) monitoring effectively captured this three-stage evolution, providing complementary evidence at different scales. In the initial adsorption stage, the negative Δf shift and positive ΔD increase in QCM-D indicated monolayer formation via electrostatic anchoring, while the decaying OIRD signal reflected the corresponding reduction in interfacial dielectric constant as

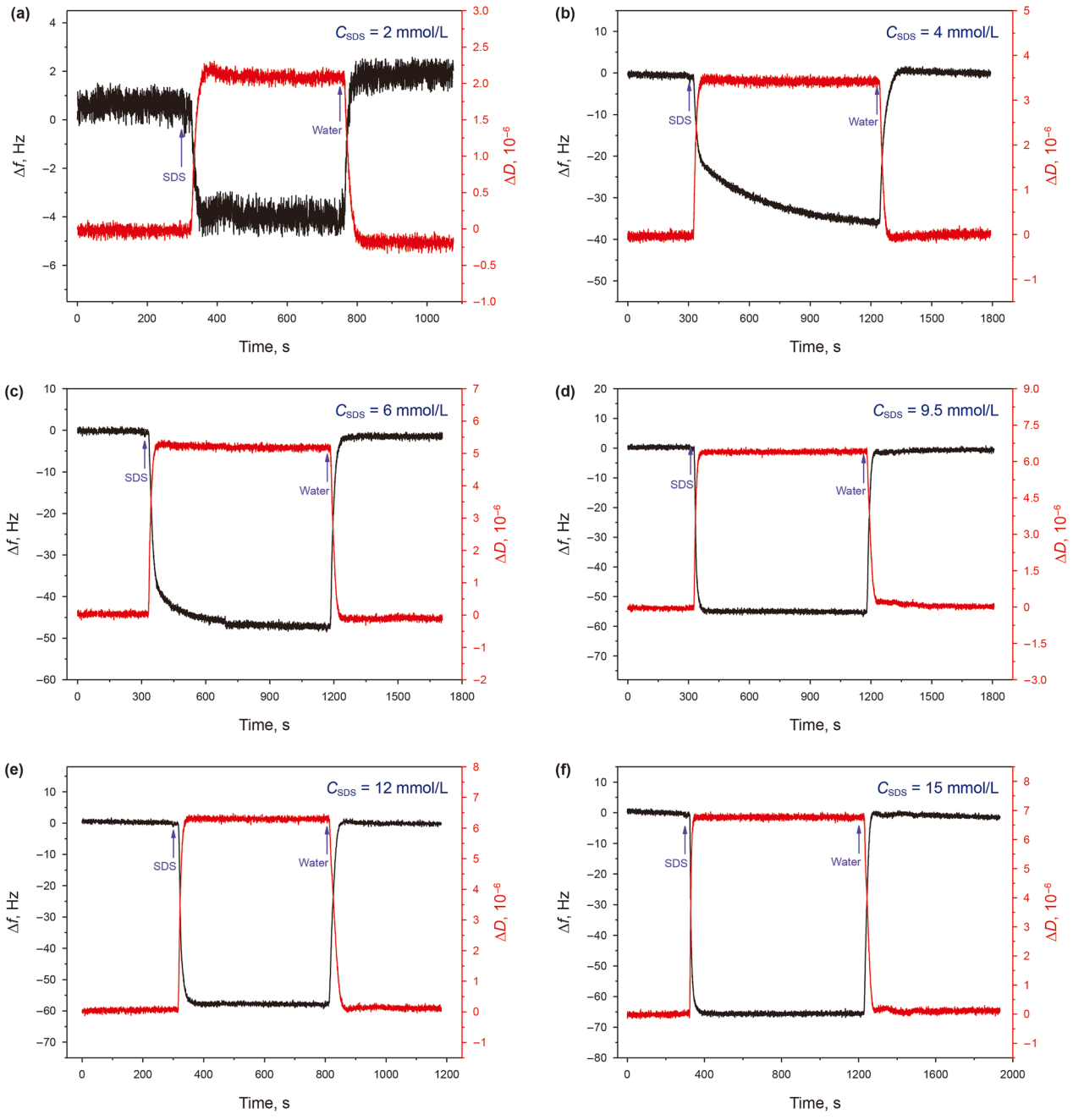

Fig. 6. QCM-D monitoring of SDS adsorption on a silica surface. Changes in Δf and ΔD over time for CTAB solutions at concentrations of 2 (**a**), 4 (**b**), 6 (**c**), 9.5 (**d**), 12 (**e**), and 15 (**f**) mmol/L, respectively. The arrows indicate the injection points for each concentration and the subsequent switch to ultrapure water for rinsing.

hydrophobic tails oriented outward. This configuration led to a marked increase in contact angle (Fig. 3(b)). During the adsorption saturation to pre-micelle formation stage, both techniques showed signal stabilization, with QCM-D confirming saturated monolayer coverage and OIRD indicating a stable, low-dielectric interface maintaining the hydrophobic state. Upon entering the post-micelle formation stage, QCM-D detected a dramatic structural transition through substantial increases in Δf and ΔD, while OIRD concurrently captured the anomalous signal increase—direct evidence of adsorption layer thickening where the thickness effect superseded dielectric changes. This coordinated nanoscale reorganization, revealed by both techniques, immediately triggered macroscopic wettability reversal, rapidly reducing the contact angle (Fig. 3(b)). The highly irreversible nature of CTAB adsorption, evidenced by minimal signal recovery in both QCM-D and OIRD upon rinsing, confirmed the exceptional stability of the electrostatically anchored primary monolayer and the subsequently formed bilayer structure. In summary, by integrating macroscopic wettability, bulk solution properties, and nanoscale interfacial dynamics, this work revealed that the headgroup charge is the decisive factor governing the bifurcation in adsorption pathways and wettability evolution of surfactants on charged mineral surfaces. CTAB, by virtue of its charge complementarity, achieved a structural evolution from an electrostatic monolayer to a hydrophobically driven bilayer, thereby exhibiting a non-monotonic, switch-like wettability reversal capability. In contrast, SDS was

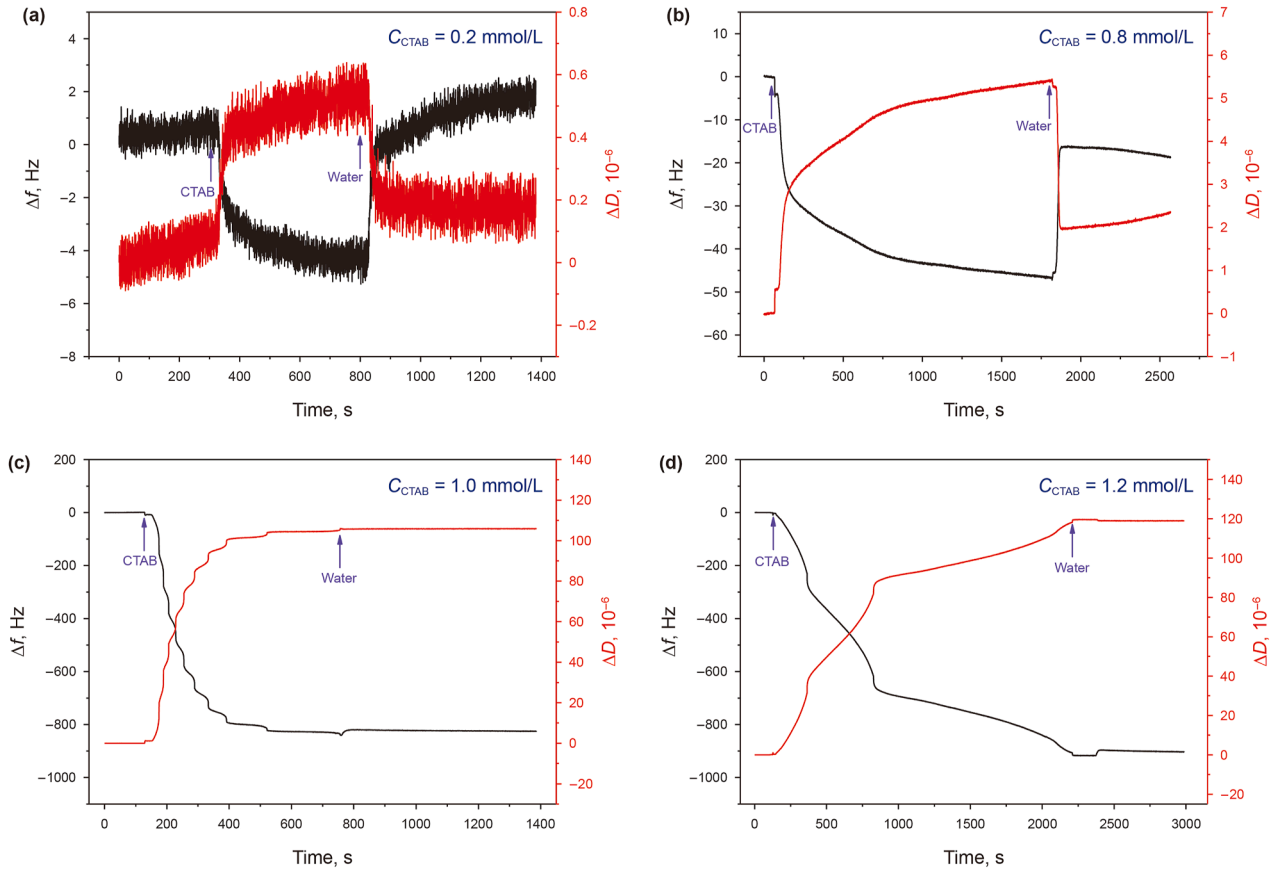

Fig. 7. QCM-D monitoring of CTAB adsorption on a silica surface. Temporal changes in frequency Δ*f* and Δ*D* in response to CTAB solutions at concentrations of 0.2 (**a**), 0.8 (**b**), 1.0 (**d**), and 1.2 (**e**) mmol/L, respectively. The arrows indicate the point of injection for each concentration and the subsequent switch to ultrapure water rinsing.

confined to simple, reversible monolayer adsorption due to charge repulsion, only capable of inducing monotonic hydrophilization.

Wettability governs the flow characteristics and distribution of fluids within reservoir rocks (Alvarez and Schechter, 2016). Modifying the wettability of crude oil reservoirs from oil-wet to water-wet can significantly enhance oil recovery. Researchers (Jarrahian et al., 2012; Li et al., 2023) have employed diverse methodologies to investigate the mechanism by which cationic surfactants alter the wettability of oil-wet surfaces. Their results indicate that the cationic surfactant CTAB forms ion pairs with carboxylic acid components present in crude oil. These ion pairs subsequently desorb from the rock surface, exposing a clean, water-wet substrate. Other studies (Kalam et al., 2021; Kharazi et al., 2023; Mohammed and Babadagli, 2015; Zamani et al., 2024) have analyzed surfactant adsorption mechanisms during surfactant flooding processes in both sandstone and carbonate reservoirs. The maximum adsorption of surfactants onto reservoir rock surfaces occurs at the CMC, with adsorption increments above the CMC being negligible. The extent of adsorption is dependent on pH and the ionic strength at the reservoir surface interface. The adsorption of surfactants onto rock surfaces, primarily driven by electrostatic interactions and van der Waals forces, modulates the solid surface energy and thereby alters the thermodynamic equilibrium at the three-phase contact line in accordance with Young's equation, leading to the observed wettability transition from hydrophobic to hydrophilic states (Kharazi et al., 2023). This study innovatively employed highly sensitive optical interfacial reflection-difference (OIRD) technology, combined with contact angle measurement, interfacial rheology, and quartz crystal microbalance with dissipation monitoring (QCM-D), to establish a multi-parameter collaborative analysis framework spanning from macro to nanoscale. The research commenced with quantitative macroscopic wettability data provided by contact angle measurements, which served as the initial benchmark and validation, revealing distinctly different wettability evolution pathways for anionic SDS and cationic CTAB. Interfacial rheology precisely determined the critical micelle concentration (CMC), providing a crucial reference for concentration-dependent studies. Building on this, OIRD and QCM-D served as core complementary techniques for unveiling the microscopic mechanisms: OIRD, with its sub-nanometer longitudinal resolution (< 1 nm), enabled, for the first time, nanoscale resolution of the adsorption kinetics of both anionic and cationic surfactants on mica, proposing a dynamic "dielectric constant-adsorbed layer thickness" competition mechanism. It elucidated that the anomalous OIRD signal enhancement originated from a micelle-induced thickening effect. QCM-D characterized the adsorbed mass, thickness evolution, and structural rigidity by monitoring changes in frequency and dissipation. The results demonstrated that cationic CTAB induced bilayer/micellar adsorption via charge reversal, leading to a non-monotonic hydrophobic-hydrophilic transition (a sharp 25° contact angle decrease post-CMC), whereas anionic SDS exhibited only monotonic hydrophilic enhancement. Building upon the multi-scale framework that correlates macroscopic wettability, bulk solution properties, and nanoscale interfacial dynamics to elucidate headgroup charge-dominated adsorption mechanisms, our future work will systematically investigate the synergistic effects of

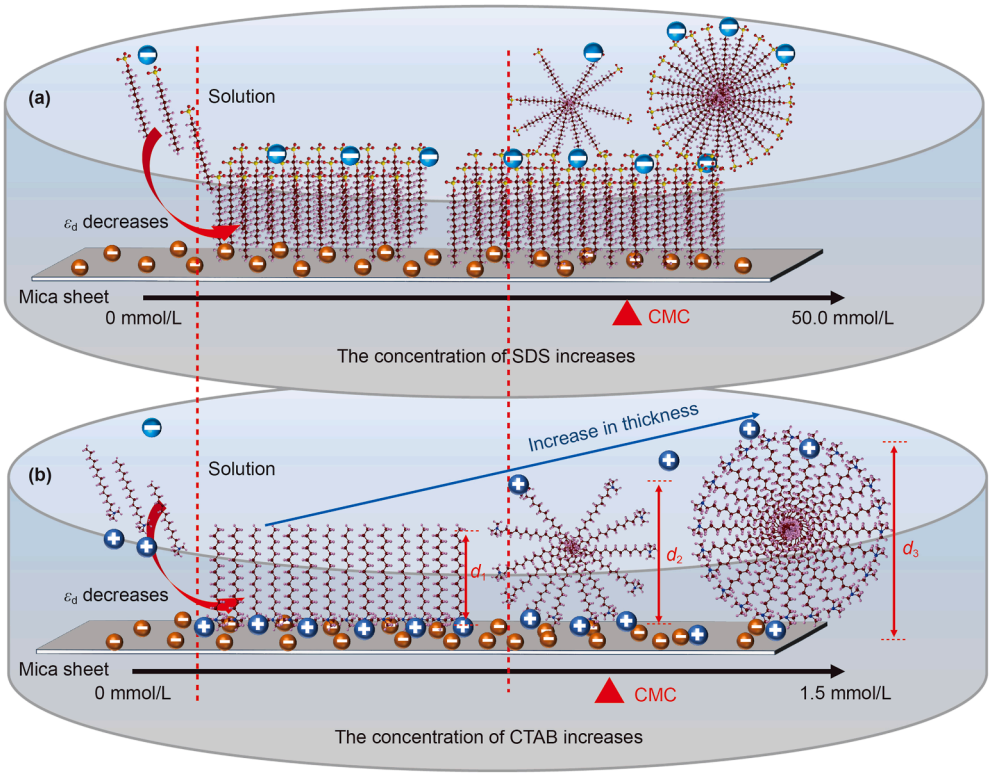

Fig. 8. Schematic diagrams contrasting the charge-dependent wettability alteration mechanisms of anionic and cationic surfactants on mica: (**a**) mechanism of SDS inducing monotonic hydrophilization, (**b**) mechanism of CTAB inducing non-monotonic wettability evolution.

temperature and salinity on interfacial surfactant/polymer nanostructure. This research direction will extend the framework's application to guide the optimization of chemical formulations for high-temperature and high-salinity reservoirs, while further establishing its paradigm-shifting potential for designing intelligently responsive interfacial materials across microfluidics, bioinspired coatings, and enhanced oil recovery.

4. Conclusions

Anionic SDS induces monotonic hydrophilization of mica, progressively reducing contact angles through tail-anchored monolayer adsorption. In contrast, cationic CTAB drives a non-monotonic transition: initial hydrophobization (increasing contact angles via headgroup-anchored monolayers) followed by abrupt hydrophilic reversal above its CMC, enabled by charge inversion and bilayer/micellar adsorption that exposes hydrophilic headgroups.

High-resolution OIRD analysis reveals a dynamic competition between interfacial dielectric constant (ε_d) and adsorption layer thickness (d). SDS adsorption is dominated by ε_d reduction, while CTAB exhibits dual-phase regulation: low-concentration ε_d decay transitions to d-dominated thickening above CMC (adsorption layer expands from ~3 to ~6 nm). This thickness-driven transition directly triggers CTAB's wettability reversal.

The divergence in adsorption behavior stems fundamentally from surfactant-substrate charge complementarity. CTAB's cationic headgroups enable strong electrostatic anchoring to negatively charged mica, facilitating dense monolayer formation and subsequent bilayer transition. SDS's anionic headgroups experience electrostatic repulsion with mica, restricting adsorption to loosely packed monolayers without structural evolution. This charge-governed adsorption dichotomy directly determines wettability outcomes.

These mechanistic insights provide molecular design principles for engineering smart interfacial materials, directly advancing optimization of enhanced oil recovery agents, microfluidic surface patterning, anti-fouling coatings, and nanofluidic systems through precise wettability control.

CRediT authorship contribution statement

Chao Song: Writing – review & editing, Writing – original draft, Methodology, Conceptualization. **Yi-Qin Yang:** Writing – original draft, Formal analysis, Data curation. **Wen-Ya Zhang:** Methodology, Formal analysis. **Xin Liu:** Methodology, Data curation. **Zhi-Yuan Xu:** Validation. **Ke-Xin Li:** Visualization, Investigation. **Hao Zhang:** Visualization, Investigation. **Chun-Qing Si:** Methodology. **Si-Hao Ma:** Visualization, Investigation. **Jia-Ning Zhang:** Visualization, Investigation. **Yan-Yan Wang:** Investigation. **Bo-Wen Sun:** Validation, Investigation. **Sheng-Nan Wu:** Investigation. **Mei-Yi Qing:** Writing – review & editing. **Qi-Chao Lv:** Writing – review & editing. **Jing Wang:** Writing – review & editing, Validation. **Hong-Lei Zhan:** Writing – review & editing, Validation, Conceptualization.

Declaration of interest statement

The authors declare that they have no known competing financial interests or personal relationships that could have appeared to influence the work reported in this paper.

Acknowledgments

This work was supported by the National Key Research and Development Project of China (2022YFC2806102) and the National Natural Science Foundation of China (Grant No. 62203079).

References

Alvarez, J.O., Schechter, D.S., 2016. Application of wettability alteration in the exploitation of unconventional liquid resources. Petrol. Explor. Dev. 43, 832–840. https://doi.org/10.1016/S1876-3804(16)30099-4.

Asadabadi, S., Saien, J., Kharazi, M., 2024. Enhanced interfacial activity by maximizing synergy between long-chain ionic liquid and conventional surfactant for enhanced oil recovery. RSC Adv. 14, 18942–18949. https://doi.org/10.1039/D4RA02092H.

Esfandyari, H., Shadizadeh, S.R., Esmaeilzadeh, F., et al., 2020. Implications of anionic and natural surfactants to measure wettability alteration in EOR processes. Fuel 278, 118392. https://doi.org/10.1016/j.fuel.2020.118392.

Ghasemlou, M., Dave, F., Ivanova, E.P., et al., 2019. Bio-inspired sustainable and durable superhydrophobic materials: From nature to market. J. Mater. Chem. A 7, 16643–16670. https://doi.org/10.1039/c9ta05185f.

Hou, B., Wang, Y., Huang, Y., 2015. Mechanistic study of wettability alteration of oil-wet sandstone surface using different surfactants. Appl. Surf. Sci. 330, 56–64. https://doi.org/10.1016/j.apsusc.2014.12.185.

Hou, B., Jia, R., Fu, M., et al., 2019. Mechanism of wettability alteration of an oil-wet sandstone surface by a novel cationic gemini surfactant. Energy & Fuels 33, 4062–4069. https://doi.org/10.1021/acs.energyfuels.9b00304.

Huang, H., Guo, M., Wu, C., et al., 2023. Lattice Boltzmann study on the effects of surface nanostructure on wettability with application in laser scanning fabrication of superhydrophobic surfaces. Sci. China Technol. Sci. 66, 3197–3205. https://doi.org/10.1007/s11431-023-2457-7.

Jarrahian, K., Seiedi, O., Sheykhan, M., et al., 2012. Wettability alteration of carbonate rocks by surfactants: A mechanistic study. Coll. Surf. Physicochem. Eng. Aspect. 410, 1–10. https://doi.org/10.1016/j.colsurfa.2012.06.007.

Kalam, S., Abu-Khamsin, S.A., Kamal, M.S., et al., 2021. Patil S. A review on surfactant retention on rocks: Mechanisms, measurements, and influencing factors. Fuel 293, 120459. https://doi.org/10.1016/j.fuel.2021.120459.

Kharazi, M., Saien, J., Torabi, M., et al., 2023. Molecular design and applications of a nanostructure green tripodal surface active ionic liquid in enhanced oil recovery: Interfacial tension reduction, wettability alteration, and emulsification. Pet. Sci. 20, 3530–3539. https://doi.org/10.1016/j.petsci.2023.07.010.

Li, H., Huang, X.B., Sun, J.S., et al., 2023. Improving the anti-collapse performance of water-based drilling fluids of Xinjiang Oilfield using hydrophobically modified silica nanoparticles with cationic surfactants. Pet. Sci. 20, 1768–1778. https://doi.org/10.1016/j.petsci.2022.10.023.

Liu, K., Vuckovac, M., Latikka, M., Huhtamäki, T., et al., 2019. Improving surface-wetting characterization. Science 363, 1147–1148. https://doi.org/10.1126/science.aav5388.

Meng, Z., Zheng, H., Qin, F., et al., 2023. Mechanistic study of the effect of hydrocarbon unsaturation on the distribution state of water molecules at the oil-water interface by oblique incident reflectance difference technique. Energy 276, 127658. https://doi.org/10.1016/j.energy.2023.127658.

Mohammed, M., Babadagli, T., 2015. Wettability alteration: A comprehensive review of materials/methods and testing the selected ones on heavy-oil containing oil-wet systems. Adv. Colloid Interface Sci. 220, 54–77. https://doi.org/10.1016/j.cis.2015.02.006.

Mousavi, S.P., Hemmati-Sarapardeh, A., Norouzi-Apourvari, S., et al., 2021. Toward mechanistic understanding of wettability alteration in calcite and dolomite rocks: The effects of resin, asphaltene, anionic surfactant, and hydrophilic nano particles. J. Mol. Liq. 321, 114672. https://doi.org/10.1016/j.molliq.2020.114672.

Pal, S., Mushtaq, M., Banat, F., et al., 2018. Review of surfactant-assisted chemical enhanced oil recovery for carbonate reservoirs: Challenges and future perspectives. Pet. Sci. 15 (1), 77–102. https://doi.org/10.1007/s12182017-0198-6.

Qing, M., Liu, J., Huang, Q., et al., 2022. In situ probing of wax precipitation of waxy oil using oblique-incidence reflectivity difference at open bulk surface. Fuel 316, 123436. https://doi.org/10.1016/j.fuel.2022.123436.

Ratanpara, A., Kim, M., 2023. Wettability alteration mechanisms in enhanced oil recovery with surfactants and nanofluids: A review with microfluidic applications. Energies 16, 8003. https://doi.org/10.3390/en16248003.

Roldán-Carrillo, T., Castorena-Cortes, G., Salazar Castillo, R.O., et al., 2023. Hybrid low salinity water and surfactant process for enhancing heavy oil recovery. Petrol. Explor. Dev. 50, 1466–1477. https://doi.org/10.1016/s1876-3804(24)60480-5.

Saien, J., Shokri, B., Kharazi, M., 2023. Synergism in mixtures of nano benzimidazolium Gemini ionic liquid and sodium dodecyl sulfate surfactants in tuning interfacial properties of crude oil−water system. J. Mol. Liq. 391, 123280. https://doi.org/10.1016/j.molliq.2023.123280.

Samiei, N.M., Wood, D.A., Sadatshojaei, E., et al., 2021. New insight to experimental study of ionic solutions with a non-ionic surfactant on wettability, interfacial tension and micro-model flooding. Fuel 285, 119126. https://doi.org/10.1016/j.fuel.2020.119126.

Sbragaglia, M., Benzi, R., Biferale, L., et al., 2006. Surface roughness-hydrophobicity coupling in microchannel and nanochannel flows. Phys. Rev. Lett. 97 (20), 204503. https://doi.org/10.1103/PhysRevLett.97.204503.

Shi, Y., Mohanty, K.K., Leung, J.Y., et al., 2024. A new mechanistic model for wettability-altering surfactant floods in carbonates. SPE J. 29, 2672–2685. https://doi.org/10.2118/219468-PA.

Wang, Y., Yang, S., Zhang, J., et al., 2023. Scalable and switchable CO_2-responsive membranes with high wettability for separation of various oil/water systems. Nat. Commun. 14 (1), 1108. https://doi.org/10.1038/s41467-023-36685-9.

Wang, Y., Sun, Y., Xue, Y., et al., 2024. Functional surfaces with reversibly switchable wettability: Fundamentals, progresses, applications and challenges. Prog. Org. Coating 188, 108167. https://doi.org/10.1016/j.porgcoat.2023.108167.

Yao, Y., Wei, M., Kang, W., 2021. A review of wettability alteration using surfactants in carbonate reservoirs. Adv. Colloid Interface Sci. 294, 102477. https://doi.org/10.1016/j.cis.2021.102477.

Zamani, A.M., Moslemi, A., Hassani, K., 2024. Experimental investigation into effects of the natural polymer and nanoclay particles on the EOR performance of chemical flooding in carbonate reservoirs. Pet. Sci. 21, 951–961. https://doi.org/10.1016/j.petsci.2023.11.001.

Zhang, B., Rane, K., Piri, M., et al., 2023. Impact of surface roughness, surface charge, and temperature on sandstone wettability alteration by nanoparticles. Pet. Sci. 20, 2852–2863. https://doi.org/10.1016/j.petsci.2023.04.004.

Zhang, J.W., Zeng, H.B., 2021. Intermolecular and surface interactions in engineering processes. Engineering 7 (1), 63–83. https://doi.org/10.1016/j.eng.2020.08.017.

Zhang, S., Huang, J., Chen, Z., et al., 2017. Bioinspired special wettability surfaces: From fundamental research to water harvesting applications. Small 13 (3), 1602992. https://doi.org/10.1002/smll.201602992.

Zhao, F., Du, Y., Yang, P., et al., 2005. Adsorption behavior of hexadecyltrimethylammonium bromide (CTAB) to mica substrates as observed by atomic force microscopy. Sci. China, Ser. B: Chem. 48 (2), 101–106. https://doi.org/10.1360/04YB0122.

Zhu, X.D., 2004. Oblique-incidence optical reflectivity difference from a rough film of crystalline material. Phys. Rev. B 69 (11), 115407. https://doi.org/10.1103/PhysRevB.69.115407.